energies

MDPI

Article

Inner Selective Non-Catalytic Reduction Strategy for Nitrogen Oxides Abatement: Investigation of Ammonia Aqueous Solution Direct Injection with an SI Engine Model

Fengshuo He [1,2], Xiumin Yu [1,2,*], Yaodong Du [1,2], Zhen Shang [1,2], Zezhou Guo [1,2], Guanting Li [1,2] and Decheng Li [1,2]

1 State Key Laboratory of Automotive Simulation and Control, Jilin University, Changchun 130022, China
2 College of Automotive Engineering, Jilin University, Changchun 130022, China
* Correspondence: yuxm@jlu.edu.cn; Tel.: +86-0431-85095897

Received: 17 June 2019; Accepted: 15 July 2019; Published: 17 July 2019

Abstract: This study contributes to a method based on an aqueous solution of ammonia direct injection for NO_x emissions control from internal combustion engines. Many previously published studies about deNO_x technology are based on selective catalytic reduction (SCR), but only few deal with inner selective non-catalytic reduction (inner SNCR) technology, which is an intensive improvement of selective non-catalytic reduction (SNCR) applied in the in-cylinder purification procedure. Before numerical calculations were carried out, the computational fluid dynamic (CFD) simulation model was validated with steady-state experimental results. The main results revealed that with the increasing concentration of aqueous solution of ammonia, nitrogen oxides gradually decrease, and the largest decline of NO_x is 65.1% with little loss of cylinder peak pressure. Unburned hydrocarbon (UHC) and carbon monoxide (CO) may increase using inner SNCR, and soot emissions show a decreased tendency. However, there is little change when ammonia content varies. Ulteriorly, refining the direct injection phase is of great help to inner SNCR technology to enhance the reduction of NO_x and reduce NH_3 oxidation and NH_3 slipping.

Keywords: deNO_x technology; inner selective non-catalytic reduction; aqueous solution of ammonia; computational fluid dynamics; combined injection

1. Introduction

The Volkswagen emissions scandal once again attracts people's attention to automobile exhaust emissions, especially NO_x emissions. With the emission regulations becoming more and more stringent, exhaust treatment technologies for engines need to be upgraded and adjusted. As common technical routes to reduce NO_x emissions, two schemes are often mentioned: water injection or water fuel emulsion and selective catalytic reduction (SCR) [1–5]. In this section, these two schemes are briefly reviewed and an innovation scheme is put forward.

Much of the literature shows that both water injection and water emulsion will enhance fuel conversion efficiency and promote NO_x emission reduction [6,7]. Parlak et al. [8] developed an electronic controlled steam injection system in the intake manifold for an spark ignition (SI) engine. In the experimental results, it is seen that the engine torque and the effective power increase up to 4.65% at 3200 rpm, specific fuel consumption reduces up to 6.44% at 2000 rpm, and NO emissions reduces 40% on average at 2800 rpm. Yang et al. [9] conducted a detailed experimental study to evaluate the effect of 10% water emulsion diesel on engine performance and emissions. The result shows that lower exhaust gas temperature and lower NO emissions are achieved at all load and engine speed condition for 10%

water emulsion diesel as compared with diesel fuel. Adnan et al. [10] conducted an experimental investigation on the optimum water injection timing for power augmentation and emission control of a hydrogen fueled compression ignition (HFCI) engine. The results show that a longer injection duration introduces more water droplets into the cylinder, reducing the in-cylinder charge temperature, which leads to NO_x reduction. Although, the amount of water by injecting or emulsifying requires special attention. Excessive water injection may lead to decreased power performance and increased incomplete combustion [11]. Thus, the NO_x emissions are limited by increasing the amount of the injected water.

SCR has been widely applied in the exhaust after-treatment device of internal combustion engines (ICE). Compared with the three-way catalytic converter (TWC), SCR is not strictly restricted by the equivalence ratio [12]. Thus, the application of SCR has more rationality and scientificity in lean burn gasoline engines and diesel engines. However, the traditional SCR technology has some blemishes, such as poor durability of SCR catalyst [13], narrow temperature window for active deNO_x [14], catalyst deactivation due to particulates accumulation [15], catalyst poisoning effect caused by heavy metals (Pb, Zn, and so on, and their oxides) [16], high cost, and difficult recovery by using the noble metal catalysts. The miniaturization and compactification of SCR equipment are also very important factors, which influence the automobile lightweight, especially the passenger car [17]. These limitations led researchers to begin to focus on selective non-catalytic reduction (SNCR), which is another technical route to reduce NO_x emissions. As a result of getting rid of the reliance on catalysts, engines with SNCR technology are less fussy about working conditions and fuel quality. Nevertheless, studies have shown that the efficient implementation of SNCR has strict requirements for the deNO_x temperature window. Nowadays, SNCR is widely applied in emissions after-treatment equipment of thermal power plants [18], but reports about SNCR applied in ICE are relatively rare [19].

Ammonia can be used as fuel surrogate for ICE or used as a reducing agent in after-treatment units for the SCR or SNCR process [20–23]. Ammonia can be easily liquefied for storage at a relatively low pressure (1.034 MPa) and ambient temperature or cooled to 240 K for storage at ambient pressure. Ryu et al. [24] performed a series experiments separately on a spark-ignition engine with ammonia blended hydrocarbon fuel and expressed their idea that a high injection pressure can increase the flow rate of the anhydrous ammonia; however, if the injection pressure is too high, ammonia will be liquefied, which has an impact on quantitative research. Meanwhile, ammonia is a double-edged sword. On one hand, as a carbon free energy storage medium, it does not produce CO_2, CO, and unburned hydrocarbon (UHC) emissions after burning [25]. On the other hand, an unreasonable supplying strategy can lead to NO_x emissions deterioration and ammonia slip [26]. Therefore, how to utilize ammonia in ICE for NO_x reduction could be an interesting issue.

It is an ideal method to add ammonia into ICE in the form of aqueous solution compared with anhydrous ammonia. $NH_3 \cdot H_2O$, the principal component of aqueous solution of ammonia, is easily decomposed to produce ammonia and water by heating. Thus, considering the coupled effect of ammonia and water for NO_x reduction may be of great significance to deNO_x. An improved $NH_3 \cdot H_2O$-SNCR process based on direct injection of aqueous solution of ammonia, namely inner selective non-catalytic reduction (inner SNCR), is proposed in this work. Comparing the inhibitory effect of pure water injection on NO_x emissions, the formation of NO_x is further inhibited by $NH_3 \cdot H_2O$-SNCR. This proposal is based on gasoline port injection (GPI) and aqueous solution of ammonia direct injection, which will contribute to mitigating NO_x emissions, as well as simplifying the layout of the after-treatment system, innovatively. The investigation on inner SNCR coupled with the numerical computational fluid dynamic (CFD) method is reinforced in this work. Previous studies of our research group [27,28] focus on combined injection technology with a dual fuel spark ignition (SI) engine, which is expediently modified for aqueous solution of ammonia direct injection when calibrating. On the basis of the goal of removing NO_x without causing other negative effects, this work will enhance understanding of the coupled effect of water and ammonia in refined CFD perspectives for reducing NO_x under the stoichiometric condition.

2. Modeling Methodology

2.1. Geometric Model and Boundary Conditions

In this work, CONVERGE software [29] with kinds of sub-models was utilized to build and calibrate the engine research model. The virtual engine was modified from a four-cylinder SI engine and the main technical parameters are shown in Table 1.

Table 1. Main technical parameters of the commercial engine.

Engine Type	Orthostichous, Four Cylinder, Water Cooled, Combined Injection
Compression ratio	9.6:1
Displacement	2.0 L
Bore × stroke	82.5 × 92.8 mm
Maximum power	147 kW (5000–6000 rpm)
Maximum torque	280 N·m (1800–5000 rpm)

On the basis of reverse engineering, a stereolithography (STL) file for a single cylinder of the commercial engine and its attachment (manifolds and valves) was obtained from 3D point clouds. Figure 1 shows the structure body (A), the surface mesh (B), and the two-dimensional section (C and D) of the structure mesh at 23 °CA after top dead centre (TDC).

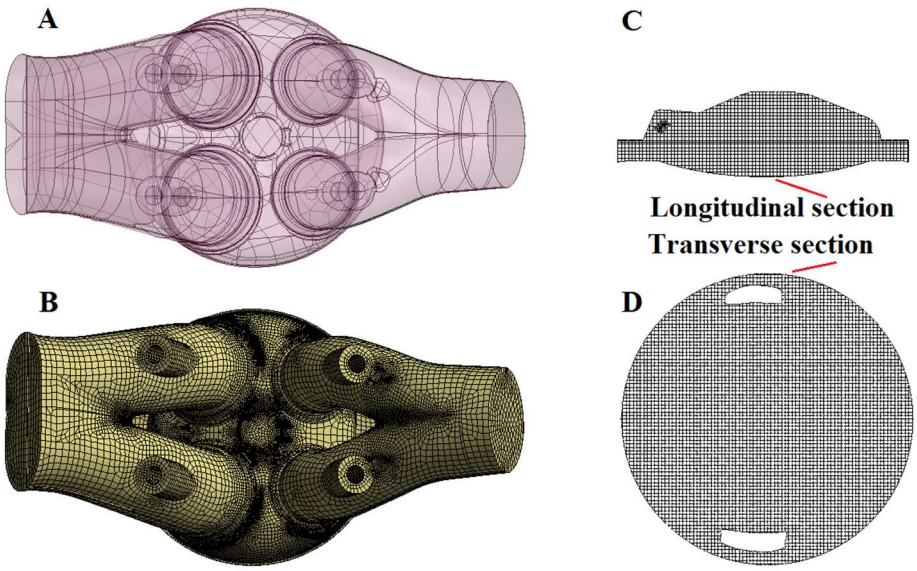

Figure 1. Structure body and mesh generation for the engine model: (**A**) STL model; (**B**) meshed model; (**C**) longitudinal section; (**D**) transverse section.

SAGE, a detailed transient chemistry solver developed by Senecal et al. [30], was chosen as the combustion model for various reaction processes. This model calculated the chemical reaction rate of each step. The more detailed the chemical reaction mechanism used in the combustion model, the closer to the actual combustion is the simulation process in the cylinder. However, in fact, the calculating speed will slow down using the detailed mechanism. Taking account of saving computational time, it is necessary to simplify the reaction mechanism according to the recorded experiment results in the previous literature.

The mechanism used in this work is composed of three parts, involving gasoline surrogate mechanism, NO_x generation mechanism, and ammonia deNO_x mechanism. The primary reference fuel (PRF) mechanism [31] including 41 species and 124 reactions is appropriate for gasoline surrogate. This PRF mechanism has been validated in a series of experiments, such as shock tube, jet stirred reactor, flow reactor, and homogeneous charge compression ignition (HCCI) engine, and it has also been widely

applied or verified in other studies [32–34]. The NO_x mechanism, a so-called extended Zeldovich mechanism, comes from Tao's work [35], which is widely referenced in published articles [36–38]. The ammonia deNO_x mechanism is collated and verified by Golovitchev [39] and it has been tested and verified as well [40,41]. This work combines these three sub-mechanisms to simulate the coupled effect of water and ammonia for the engine deNO_x process with inner SNCR strategy.

As a widely used empirical model, the Hiroyasu model was employed in the present soot prediction, which could make an all-round evaluation on the comprehensive applicability of the inner SNCR method [42]. Re-normalization group (RNG) k-ε model [43] is used for turbulence simulation. The wall heat transfer model, developed by Han and Reitz [44], is used for the wall heat loss. The Kelvin–Helmholtz and Rayleigh–Taylor (KH-RT) hybrid model [45] is used for fuel injection and spray breakup. In detail, the primary breakup is controlled by the KH model and the sub-droplets are produced in this process. The subsequent breakup is determined by the competition mechanism between KH model and RT model. It is necessary to consider turbulence in the continuous phase with the motion of oil droplets, so the O'Rourke model [46] is chosen for turbulence in this work. A spherical module with energy of 40 mJ simulates ignition by the spark plug at the side of the exhaust manifold. Figure 2 shows the relative locations of the port fuel injector, the direct injector, and the spark plug in the CFD model.

Figure 2. Relative locations of port fuel injector, direct injector, and spark plug.

2.2. Initial Parameters and Boundary Conditions

Initial parameters and boundary conditions of the engine model were mainly based on experimental measurement as well as calculation values from GT-SUITE code. For four-stroke engines, it is necessary to make it clear that 0 °CA represents the top dead centre (TDC) for firing in this investigation. Thus, the negative values mean the event happening before TDC and positive values mean the event happening after TDC. Table 2 shows the initial parameters and boundary conditions. The test fuel, gasoline with research octane number (RON) 90, was applied in the calibration based on combustion and emissions. The injected aqueous solution of ammonia was preconfigured with ammonia mass fraction (AMF) of 0%, 10%, and 20%, respectively. The direct injection (DI) timing of the aqueous solution of ammonia was set to −105 °CA, 0 °CA, and 60 °CA, respectively. All of the simulations began at −383 °CA and ended at 120 °CA. In order to facilitate and understand the comparison of the results in Section 3, the cases and the legend nomenclature are shown in Table 3.

Table 2. Initial parameters and boundary conditions. DI, direct injection; PRF, primary reference fuel; AMF, ammonia mass fraction.

Engine speed	1500 r/min
Temperature of cylinder head	550 K
Temperature of piston	600 K
Temperature of cylinder liner	450 K
Injected mass of PRF 90	44.87 mg
Injection timing of PRF 90	−373 °CA
Injected mass of the aqueous solution of ammonia	8.97 mg
DI timing of the aqueous solution of ammonia	−105 °CA, 0 °CA, and 40 °CA
NH_3 mass fraction in the aqueous solution of ammonia (AMF)	0% (pure water), 10%, and 20%
Injection pressure of the aqueous solution of ammonia	5 MPa
Intake manifold temperature/pressure	313 K/0.1 MPa
Exhaust manifold temperature/pressure	650 K/0.11 MPa
Intake valve open (IVO)	−381 °CA
Intake valve closed (IVC)	−120 °CA
Exhaust valve open (EVO)	−566 °CA
Exhaust valve closed (EVC)	−340 °CA
Global equivalence ratio	1 (stoichiometric condition)
Ignition energy	0.04 J
Ignition timing	−13 °CA

Table 3. Setting of the simulation cases and the legend nomenclature.

	Original Baseline	AMF = 0%	AMF = 10%	AMF = 20%
DI timing	Null	−105 °CA 0 °CA 40 °CA	−105 °CA 0 °CA 40 °CA	−105 °CA 0 °CA 40 °CA

2.3. Model Validation

The test experiment system for calibration is illustrated in Figure 3. Detailed information of the test equipment and its accuracy were presented in the work of [27]. In order to ensure the accuracy of the verification, the experiment and simulation were under the same working conditions, namely at the speed of 1500 r/min and at the torque of 40 N·m. Meanwhile, the overall equivalence ratio of 1 was used for the stoichiometric condition. PRF 90 (isooctane: 90% vol. and n-heptane: 10% vol.) was used to match the experimental gasoline with RON 90. Cylinder pressure, heat release rate (HRR), and global NO_x emissions were used for calibration, as shown in Figure 4.

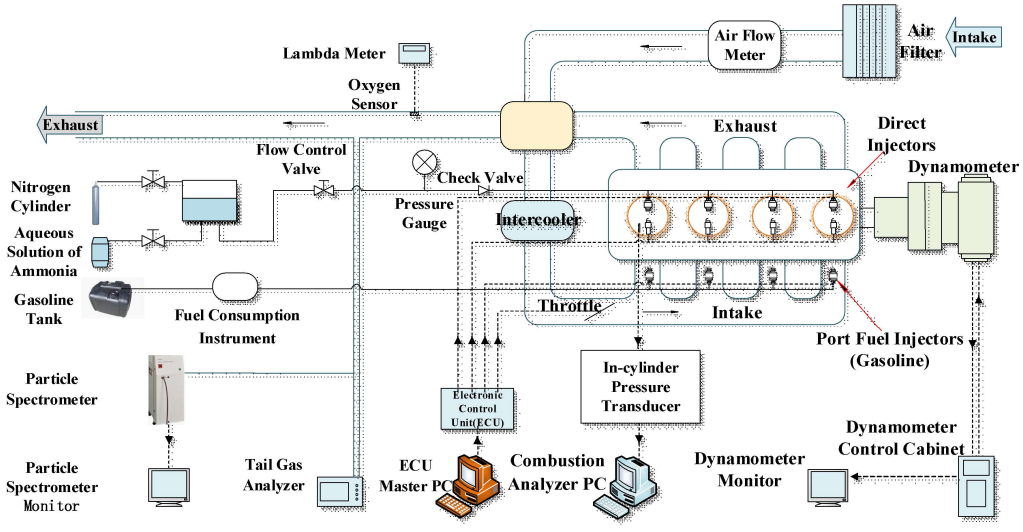

Figure 3. Engine test system.

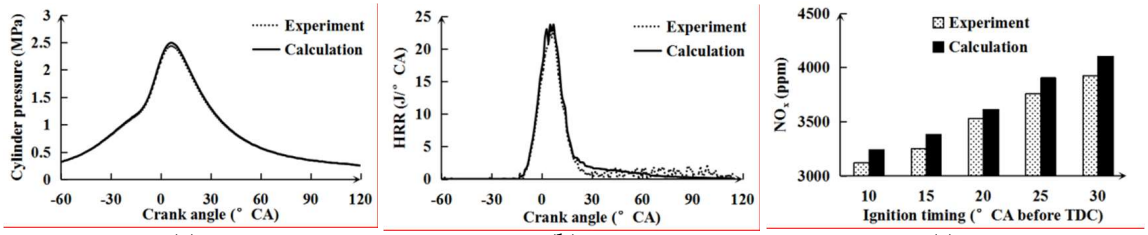

(**a**) (**b**) (**c**)

Figure 4. Comparison of calculated and measured (**a**) cylinder pressures, (**b**) heat release rates (HRRs), and (**c**) global NO_x emissions. TDC, top dead centre.

In Figure 4, the simulation results coincided with the experimental results at most coordinates. The simulation error was mainly the result of the accuracy error of heat transfer loss and the reduced PRF mechanism. Because the average error was less than 5%, the subsequent results and analysis got sufficient reliable assurance.

3. Results and Discussion

3.1. Cylinder Pressure

In Figure 5a, the DI event occurs before combustion (DI timing = −105 °CA). With AMF increasing, the peak pressure decreases first and then increases when AMF = 20%. The peak pressure change rate is −0.22%–0.37%. This is because that part of NH_3 is oxidized, compensating for the pressure drop caused by water. In Figure 5b, the DI event occurs during combustion (DI timing = 0 °CA). A significant delay (0.9 °CA) is observed. However, the pressure is without noticeable changes with the variation of AMF, which indicates no compensation for pressure by NH_3 addition. These two cases, DI timing = −105 °CA or 0 °CA, will cause lag of the phase angle corresponding to the peak pressure. Most of the components in the aqueous solution of ammonia are water, the local adiabatic flame temperature decreases in the cylinder due to the phase change of water, which is an endothermic process. Further, the temperature dropping further affects the chemical reaction rate. This is why the crank angle phase is delayed. Water direct injection could promote the formation of a highly humid air/fuel mixture, which inhibits the advance and spread of the flame front. Especially when the injection timing is near the combustion phase (DI timing = 0 °CA), it is likely to cause peak pressure decrease, peak phase angle delay, incomplete combustion, and power decrease as a result of more interference. In Figure 5c, because the direct injection happens after the combustion phase (DI timing = 40 °CA), there is no change in peak pressure and a slight fluctuation (±1.69%) occurs in cylinder pressure after 40 °CA with the variation of AMF.

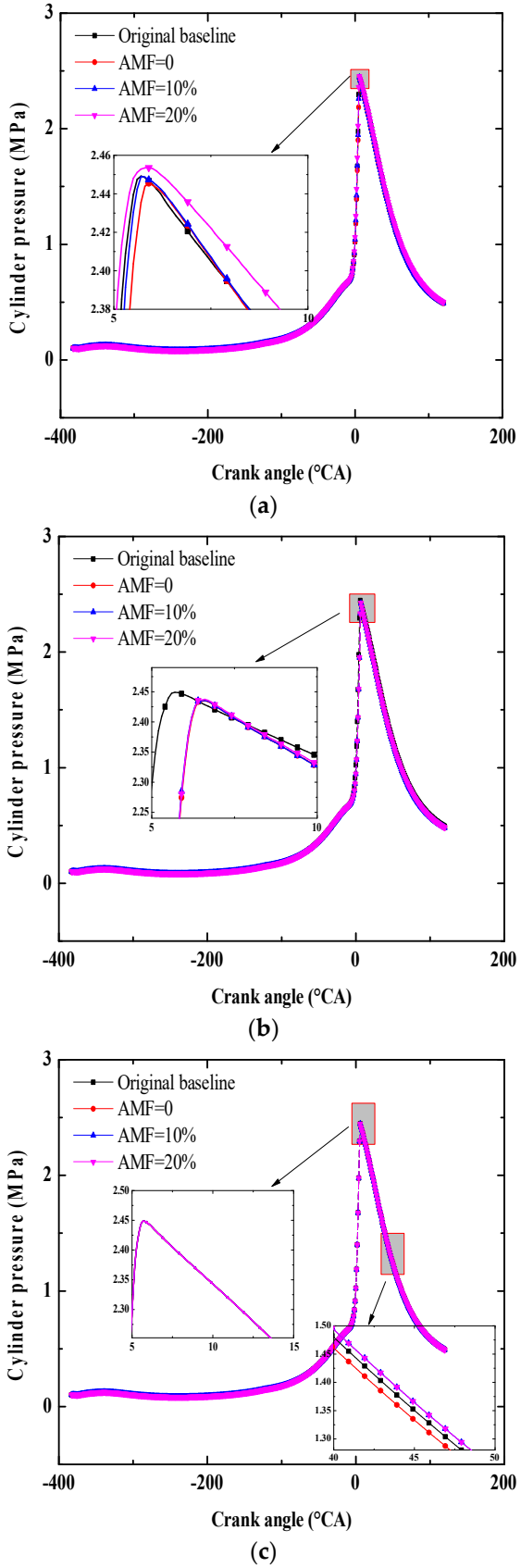

Figure 5. Cylinder pressure at different direct injection (DI) timings with variation of ammonia mass fraction (AMF): (**a**) DI timing = −105 °CA; (**b**) DI timing = 0 °CA; (**c**) DI timing = 40 °CA.

3.2. Major Intermediates Combustion Species

Variations in highly active radicals such as OH, H_2O_2, and HO_2 can be captured as a crucial indicator to reflect combustion rate and intensity [47]. Figures 6–8 show the effect of AMF on OH, H_2O_2, and HO_2 at different DI timings. When DI timing = −105 °CA, there is enough time to form a high humidity mixture before burning. This injection strategy is the same as the inlet port injection or fumigation situation. Water evaporates and absorbs heat, causing the cylinder temperature decrease. Meanwhile, there is a lag in the peak concentration of all species. The hysteresis effect of combustion is inhibited with the increase of ammonia concentration. When DI timing = 0 °CA, the hysteresis is reduced and combustion phase does not change further with variation of AMF. When DI timing = 40 °CA, water (AMF = 0) or aqueous solution of ammonia (AMF = 10% and 20%) injection occurs after combustion phase and most of the curves overlap in different AMF in Figures 6c, 7c and 8c, which indicates very little effect in combustion using inner SNCR. OH has been identified as a marker of combustion occurrence in many literature studies [48–51]. H_2O_2 and HO_2 also play an important role in high temperature reaction process through #1~#6, which are highly susceptible to water addition, especially causing temperature drop and reaction delay.

$$\#1: C_7H_{16} + O_2 = C_7H_{15} + HO_2$$

$$\#2: C_8H_{18} + O_2 = C_8H_{17} + HO_2$$

$$\#3: C_7H_{16} + HO_2 = C_7H_{15} + H_2O_2$$

$$\#4: C_8H_{18} + HO_2 = C_8H_{17} + H_2O_2$$

$$\#5: HO_2 + HO_2 = H_2O_2 + O_2$$

$$\#6: H_2O_2\ (+M) = OH + OH\ (+M)$$

3.3. Major NO_x Emissions

Most NO_x emissions exist in the form of NO in engine cylinders [52,53]. Thus, this fundamental research takes NO as the representative of NO_x to evaluate the proposed inner SNCR method. Figures 9–11 exhibit the mole fraction evolution of NO emissions in the transverse section of the combustion room under stoichiometric condition at three DI timings.

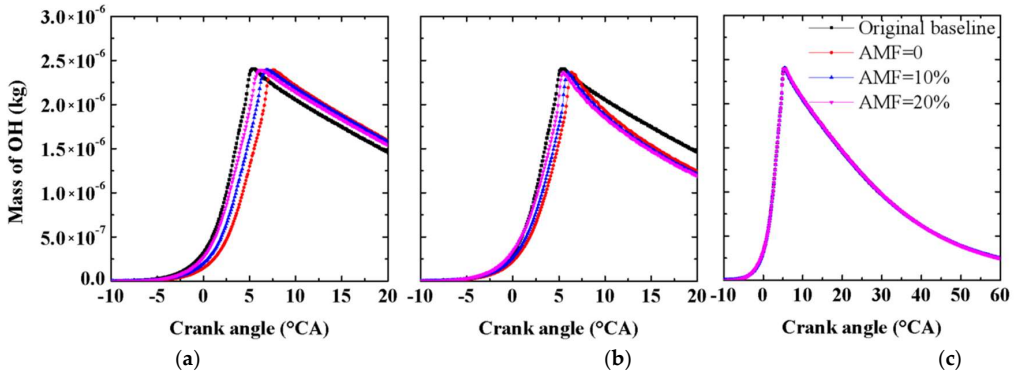

Figure 6. Mass of OH radicals at different DI timings with variation of AMF: (**a**) DI timing = −105 °CA; (**b**) DI timing = 0 °CA; (**c**) DI timing = 40 °CA.

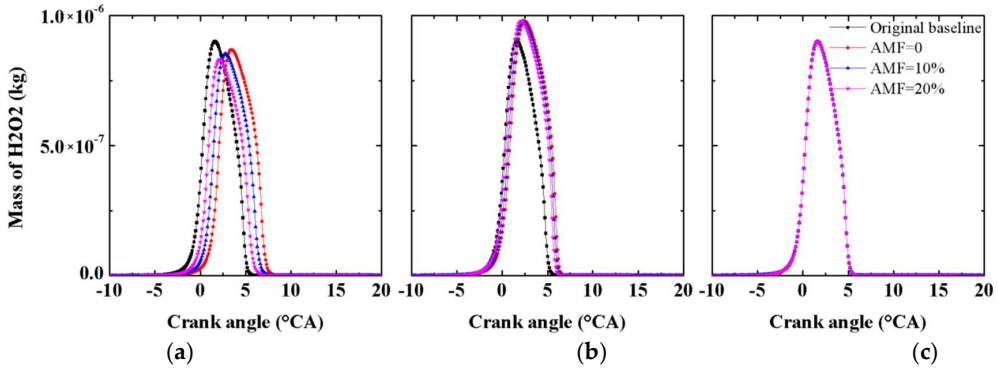

Figure 7. Mass of H_2O_2 radicals at different DI timings with variation of AMF: (**a**) DI timing = −105 °CA; (**b**) DI timing = 0 °CA; (**c**) DI timing = 40 °CA.

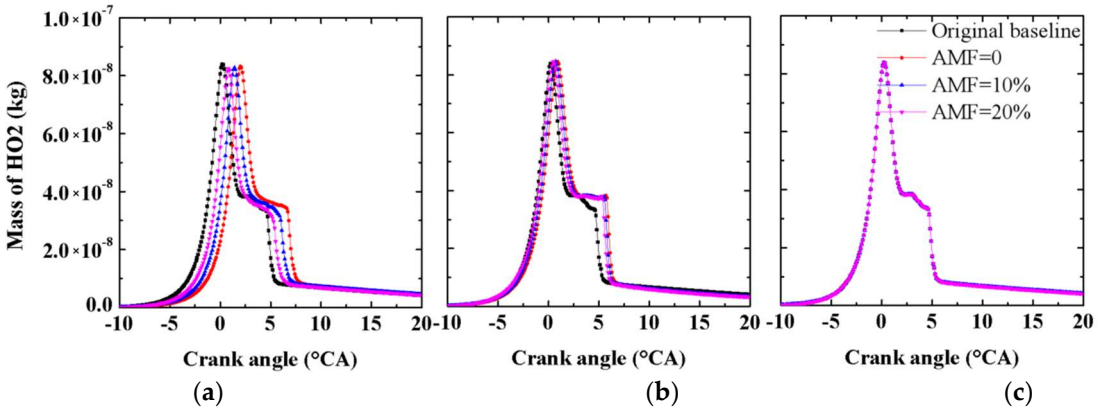

Figure 8. Mass of HO_2 radicals at different DI timings with variation of AMF: (**a**) DI timing = −105 °CA; (**b**) DI timing = 0 °CA; (**c**) DI timing = 40 °CA.

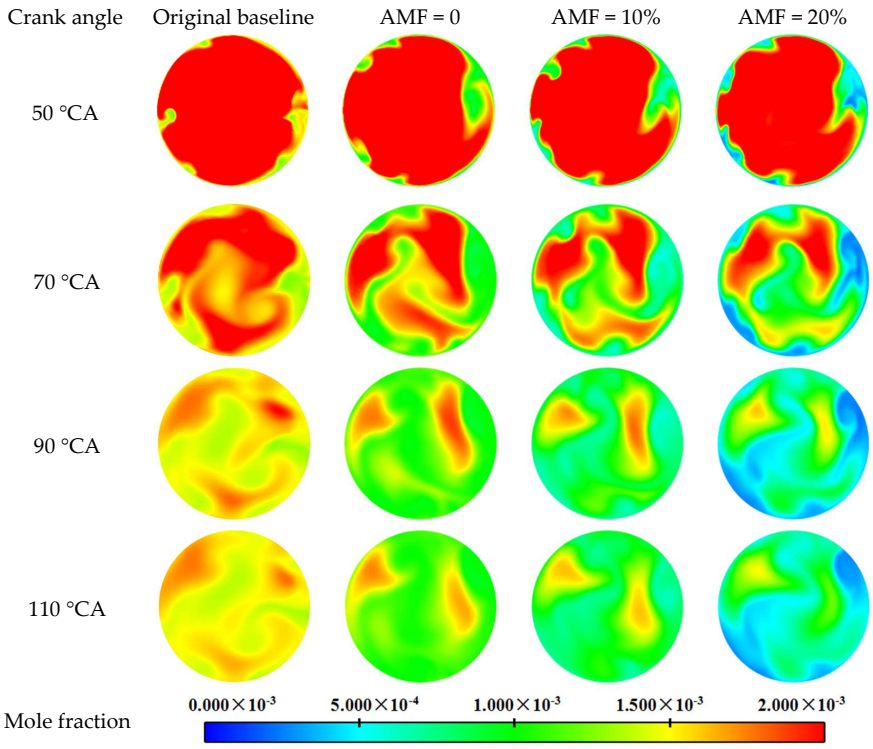

Figure 9. NO evolution with variation of AMF (DI timing = −105 °CA).

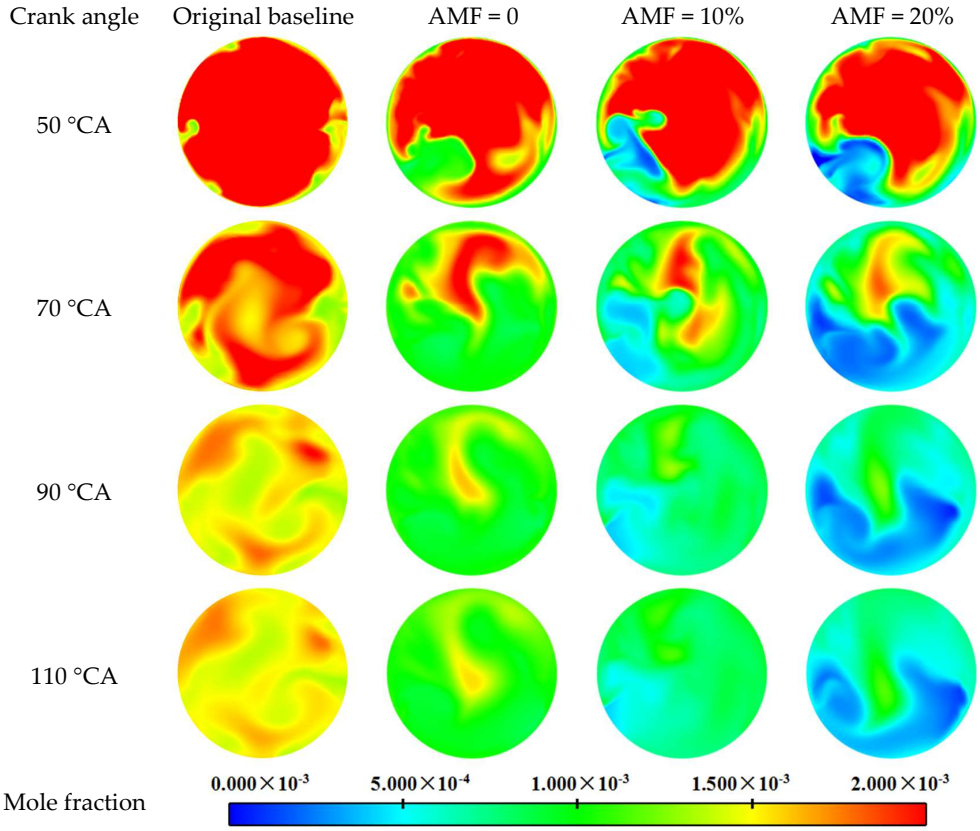

Figure 10. NO evolution with variation of AMF (DI timing = 0 °CA).

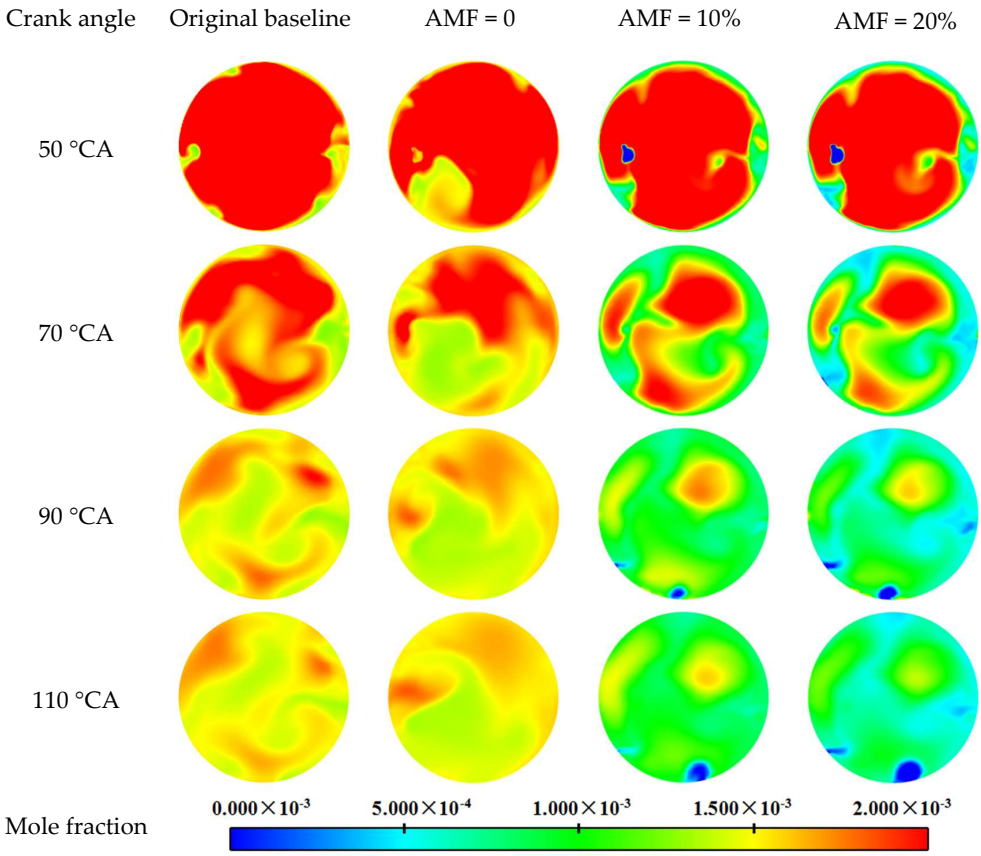

Figure 11. NO evolution with variation of AMF (DI timing = 40 °CA).

In order to fully compare the evolution of NO emissions with different DI timings, the image post-processing of the calculated results starts from 50 °CA and ends at 110 °CA. Again, the original baseline represents the NO emissions of the prototype engine without inner SNCR and the AMF value represents the different ammonia concentration in the aqueous solution of ammonia. When AMF = 0, namely pure water injection, the NO emissions show a clear decreasing trend compared with the original baseline in Figures 9–11. This can be easily explained that the water injection reduces the in-cylinder temperature and the lower flame temperature inhibits the formation of NO_x. On the basis of the theory from Zeldovich [54], thermal NO_x production doubles for every 90 K temperature increase when the flame temperature is above 2000 K. Therefore, it can be seen that these results conform to Zeldovich mechanism with different DI timings using water injection method, and similar conclusions appear in the literature [55–57]. With the increase of ammonia concentration, the regional concentration of NO obviously shrinks in these three figures, which is because high concentration aqueous solution of ammonia contributes to perfect NO reduction. For DI timing, the retention time of aqueous solution of ammonia in the combustion chamber is longer when DI timing is earlier, so NO emissions performance of DI timing = −105 °CA is better than that of DI timing = 40 °CA. Additionally, when DI timing = 40 °CA, poor diffusion of ammonia slows down NO reduction, so the final NO concentration is still at a high level. Particularly, DI timing = 0 °CA achieved better NO emissions effect than DI timing = −105 °CA and DI timing = 40 °CA. This is mainly because the DI timing (0 °CA) is close to the ignition timing (−13 °CA), which causes greater disturbance and temperature drop at the front of the flame. The consequence is that the peak cylinder pressure and active ingredients are sacrificed, as shown in Figures 5b and 6b. In order to demonstrate the effect of $deNO_x$ with the inner SNCR method, compared with the original baseline, Table 4 is calculated and recorded based on the data at the end of the simulation (120 °CA).

Table 4. Decrease of NO emissions with variation of DI timing and AMF based on original values.

	AMF = 0%	**AMF = 10%**	**AMF = 20%**
DI timing = −105°CA	37.4%	45.7%	54.0%
DI timing = 0 °CA	48.6%	56.9%	65.1%
DI timing = 40 °CA	20.3%	27.1%	33.6%

3.4. Other Emissions

Figures 12–14 show the recorded data at the end of the CFD simulation (120 °CA). As shown in Figure 12, compared with the original values, SNCR technology tends to increase UHC, and the maximum increment is 27.6%; whereas with the increase of ammonia concentration, slightly UHC is suppressed. For most ICE, the wall quenching and the slit effect may deteriorate UHC emissions. In this work, however, the result above is mainly because the mass of the aqueous solution injected in the combustion room is constant. Therefore, the increase of ammonia will inevitably lead to the decrease of water, which is the main deteriorator of UHC. When DI timing = 0 °CA, severe flame interference and heat transfer barriers promote larger generation of UHC than that when DI timing = −105 °CA and 40 °CA. As an additional confirmation for the effect of aqueous solution, Lanzanova pointed that increased air dilution reduces the combustion temperature and lowers post-flame UHC oxidation [58].

In Figure 13, the change of CO concentration is similar to UHC with the variation of DI timing, although their formation mechanism is essentially different. The biggest change took place in DI = 0 and AMF = 20%, with a maximum increase of 15.3%. For incomplete combustion products, inert substances direct injection hinders flame development. On the one hand, the reaction formula, $CO + OH = CO_2 + H$, is the key reaction pathway for CO oxidation to CO_2 [59]. On the basis of Figure 6b, an obvious OH decline occurred as aqueous solution was injected, and this inhibits the above-mentioned positive reaction process. On the other hand, a part of ammonia may react with oxygen to produce NO_x under high temperature, resulting in local oxygen deficiency, which increases

incomplete oxidation of the hydrocarbon fuel. Generally, increase in ammonia concentration leads to a slight increase in CO in these three DI timings.

In Figure 14, there is no obvious soot fluctuation compared with the original baseline (calibrated value), which means that the inner SNCR method maintained good soot tolerance for the addition of ammonia aqueous solution at different DI strategies. When DI timing = −105 °CA and 0 °CA. The earlier DI timing inhibits the formation of soot, mainly as a result of the inhibition mechanism of aqueous solution on high temperature. The maximum reduction is 16.9%. When DI timing = 40 °CA, the DI method of aqueous solution of ammonia plays little effect on soot formation or consumption.

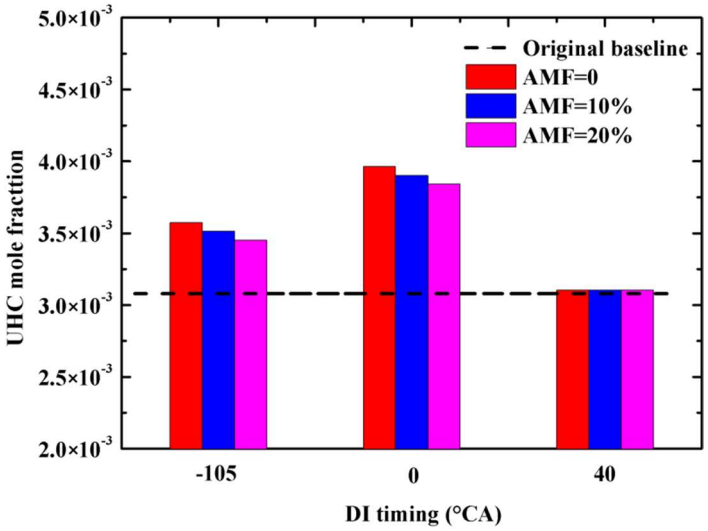

Figure 12. UHC variation at different DI timings and AMF values.

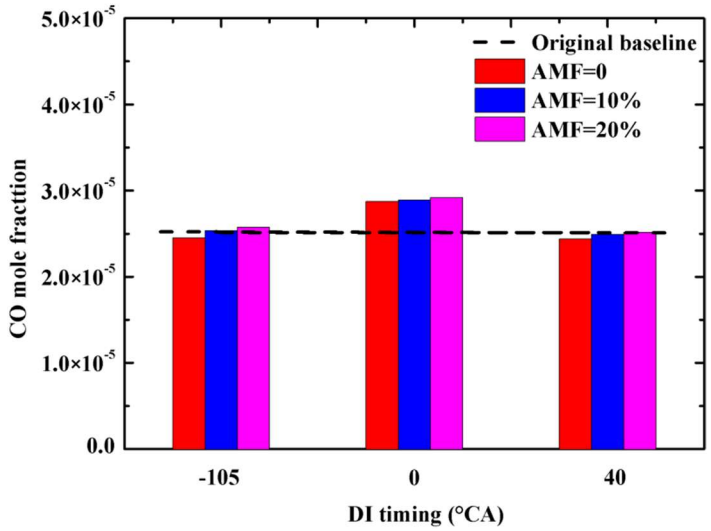

Figure 13. CO variation at different DI timings and AMF values.

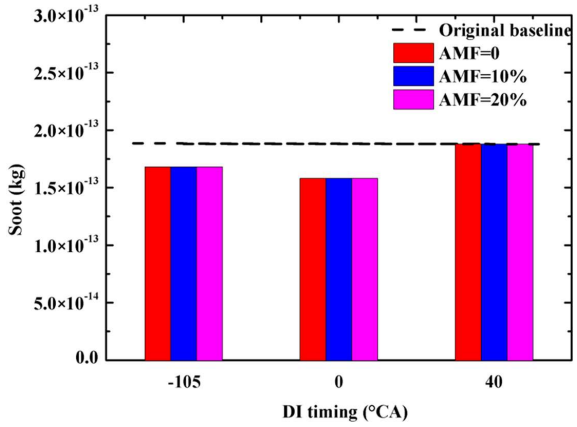

Figure 14. Soot variation at different DI timings and AMF values.

3.5. Contribution of Ammonia

In this work, ammonia was introduced to promote the reduction of NO_x on the basis of in-cylinder water direct injection. By counting the types of ammonia reactions in each cell, contribution of NH_3 were obtained. In Figure 15, two concentrations (AMF = 10% and 20%) and three DI timings (DI timing = −105 °CA, 0 °CA, and 40 °CA) are analyzed. Additionally, the contribution of ammonia is divided into three parts, for reduction ($NH_3 + NO \rightarrow N_2 + H_2O$), oxidation ($NH_3 + O_2 \rightarrow NO + H_2O$), and slipping (not involved in any reactions). It is beneficial to analyze the proportion of different effects to promote the positive effects of ammonia and to inhibit the negative effects of ammonia. The contribution sequence for reduction effect is case 1 > case 2 > case 3. The contribution sequence for oxidation is case 2 > case 1 > case 3. The contribution sequence for slipping is case 3 > case 2 > case 1. The above results can be analyzed as follows: contribution for reduction and slipping are mainly related to the retention time of NH_3 in the combustion chamber and an early DI timing results in longer retention time and further increases the contribution of NH_3 for reduction and decreases the contribution of NH_3 for slipping. However, an early DI timing means that more NH_3 may be oxidized to NO under high cylinder temperature, which weakens the selectivity for $deNO_x$. Additionally, the increase of ammonia composition is favorable to the enhancement of the $deNO_x$ effect, but the contribution of NH_3 for reduction is decreased. Thus, ammonia concentration is not likely to increase limitlessly, and DI timing matching the appropriate ignition phase is the best choice to play the maximum positive role of ammonia for inner SNCR.

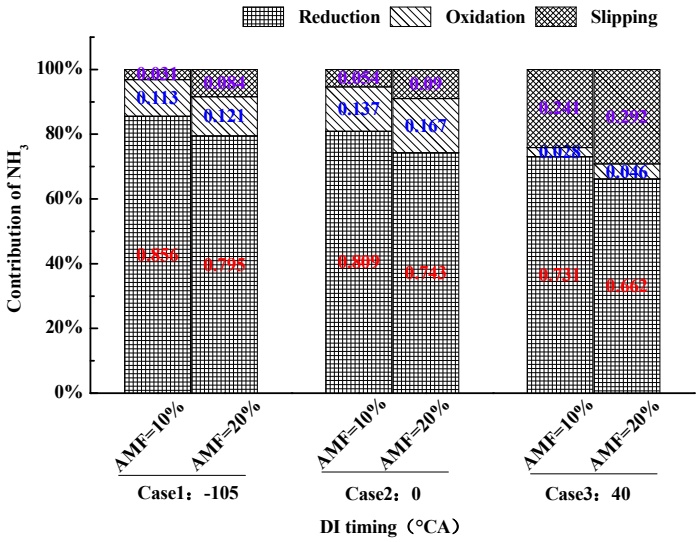

Figure 15. Contribution of ammonia.

4. Conclusions

Combining the respective characteristics of water DI technology and SNCR technology, this paper contributed to an innovation method, inner SNCR, which was verified based on CFD scheme in an SI engine model with port fuel injection and ammonia aqueous solution direct injection. A series of results with three AMF values and three DI timings were fully presented under stoichiometric condition. Some main conclusions are summarized as follows:

1. Inner SNCR, an innovate method put forward for ICE, can effectively inhibit NO_x emissions with less negative effects. More NO reduction can be achieved by NH_3 addition rather than by increasing water injection. With the increase of ammonia composition, the largest decline of NO_x is 65.1%, when DI timing = 0° CA for stoichiometric condition.
2. By using ammonia aqueous solution direct injection, the in-cylinder pressure will decrease slightly, and the corresponding phase of peak pressure will lag behind. However, owing to the small amount of injected aqueous solution (about 20% water fuel ratio), the impact on dynamic performance is very small.
3. As a relatively inert component, aqueous solution of ammonia inhibits the rapid accumulation of active radicals in the combustion chamber, which directly leads to retard of combustion reaction rate and delay of peak pressure.
4. Improper ammonia solution injection phase may cause incomplete combustion and an increase in UHC and CO emissions. The maximum increase of UHC is 27.6% and the maximum increase of CO is 15.3%. However, for soot, there is a decline when DI timing = −105 °CA and 0 °CA, and the maximum reduction is 16.9%.
5. The contribution of the ammonia addition is divided into three parts: reduction, oxidation, and slipping. The reduction effect and slipping effect are mainly related to the retention time, so an earlier DI timing helps to strengthen reduction of NO by NH_3 and reduce NH_3 slipping. Nevertheless, an early DI timing means that more NH_3 may be oxidized to NO under high cylinder temperature simultaneously.

Author Contributions: Conceptualization, F.H.; methodology, Z.S., Z.G., G.L., and D.L.; software, F.H.; validation, F.H. and Y.D.; formal analysis, F.H.; investigation, F.H.; resources, X.Y.; data curation, F.H.; writing—original draft preparation, F.H.; writing—review and editing, F.H.; visualization, F.H.; supervision, X.Y.; project administration, X.Y.; funding acquisition, X.Y.

Funding: This research was funded by the National Natural Science Foundation of China, grant number 51276079.

Acknowledgments: The authors appreciate the insightful comments and suggestions from the reviewers and the editor.

Conflicts of Interest: The authors declare no conflict of interest.

Nomenclature

NO_x	nitrogen oxides
$deNO_x$	denoxtronic
SCR	selective catalytic reduction
SNCR	selective non-catalytic reduction
CFD	computational fluid dynamic
CO_2	carbon dioxide
CO	carbon monoxide
UHC	unburned hydrocarbon
ICE	internal combustion engine
HFCI	hydrogen fueled compression ignition
TWC	three way catalytic converter
Pb	plumbum
Zn	zinc

RON	research octane number
AMF	ammonia mass fraction
DI	direct injection
HCCI	homogeneous charge compression ignition
NH_3	ammonia
H_2O	water
$NH_3{\cdot}H_2O$	ammonia monohydrate
SI	spark ignition
HRR	heat release rate
STL	stereolithography
TDC	top dead centre
PRF	primary reference fuel
PFI	port fuel injection
GPI	gasoline port injection
RNG	re-normalization group
KH-RT	Kelvin-Helmholtz and Rayleigh-Taylor
CA	crank angle
NO	nitric oxide
N_2	nitrogen
H	hydrogen atom
O_2	oxygen
C_7H_{16}	n-heptane
C_7H_{15}	n-heptane alkyl
C_8H_{18}	isooctane
C_8H_{17}	isooctane alkyl
HO_2	hydroperoxyl radical
H_2O_2	hydrogen peroxide
OH	hydroxyl radical
M	third body

References

1. Damma, D.; Ettireddy, P.R.; Reddy, B.M.; Smirniotis, P.G. A Review of Low Temperature NH_3-SCR for Removal of NO_x. *Catalysts* **2019**, *9*, 349. [CrossRef]
2. Boningari, T.; Pappas, D.K.; Ettireddy, P.R.; Kotrba, A.; Smirniotis, P.G. Influence of SiO_2 on M/TiO_2 (M = Cu, Mn, and Ce) Formulations for Low-Temperature Selective Catalytic Reduction of NO_x with NH_3: Surface Properties and Key Components in Relation to the Activity of NO_x Reduction. *Ind. Eng. Chem. Res.* **2015**, *54*, 2261–2273. [CrossRef]
3. Sreekanth, P.M.; Peña, D.A.; Smirniotis, P.G. Titania Supported Bimetallic Transition Metal Oxides for Low-Temperature SCR of NO with NH_3. *Ind. Eng. Chem. Res.* **2006**, *45*, 6444–6449. [CrossRef]
4. Boningari, T.; Koirala, R.; Smirniotis, P.G. Low-temperature catalytic reduction of NO by NH_3 over vanadia-based nanoparticles prepared by flame-assisted spray pyrolysis: Influence of various supports. *Appl. Catal. B Environ.* **2013**, *140–141*, 289–298. [CrossRef]
5. Smirniotis, P.G.; Peña, D.A.; Uphade, B.S. Low-Temperature Selective Catalytic Reduction (SCR) of NO with NH_3 by Using Mn, Cr, and Cu Oxides Supported on Hombikat TiO_2. *Angew. Chem. Int. Ed.* **2001**, *40*, 2479–2482. [CrossRef]
6. Boretti, A. Water injection in directly injected turbocharged spark ignition engines. *Appl. Therm. Eng.* **2013**, *52*, 62–68. [CrossRef]
7. Zhu, S.; Hu, B.; Akehurst, S.; Copeland, C.; Lewis, A.; Yuan, H.; Kennedy, I.; Bernards, J.; Branney, C. A review of water injection applied on the internal combustion engine. *Energy Convers. Manag.* **2019**, *184*, 139–158. [CrossRef]
8. Cesur, İ.; Parlak, A.; Ayhan, V.; Boru, B.; Gonca, G. The effects of electronic controlled steam injection on spark ignition engine. *Appl. Therm. Eng.* **2013**, *55*, 61–68. [CrossRef]

9. Fahd, M.E.A.; Wenming, Y.; Lee, P.S.; Chou, S.K.; Yap, C.R. Experimental investigation of the performance and emission characteristics of direct injection diesel engine by water emulsion diesel under varying engine load condition. *Appl. Energy* **2013**, *102*, 1042–1049. [CrossRef]
10. Adnan, R.; Masjuki, H.H.; Mahlia, T.M.I. Performance and emission analysis of hydrogen fueled compression ignition engine with variable water injection timing. *Energy* **2012**, *43*, 416–426. [CrossRef]
11. Hoppe, F.; Thewes, M.; Baumgarten, H.; Dohmen, J. Water injection for gasoline engines: Potentials, challenges, and solutions. *Int. J. Engine Res.* **2016**, *17*, 86–96. [CrossRef]
12. Matsumoto, S. Recent advances in automobile exhaust catalysts. *Catal. Today* **2004**, *90*, 183–190. [CrossRef]
13. Schmieg, S.J.; Oh, S.H.; Kim, C.H.; Brown, D.B.; Lee, J.H.; Peden, C.H.F.; Kim, D.H. Thermal durability of Cu-CHA NH_3-SCR catalysts for diesel NO_x reduction. *Catal. Today* **2012**, *184*, 252–261. [CrossRef]
14. Guan, B.; Zhan, R.; Lin, H.; Huang, Z. Review of state of the art technologies of selective catalytic reduction of NO_x from diesel engine exhaust. *Appl. Therm. Eng.* **2014**, *66*, 395–414. [CrossRef]
15. Liu, C.; Shi, J.-W.; Gao, C.; Niu, C. Manganese oxide-based catalysts for low-temperature selective catalytic reduction of NO_x with NH_3: A review. *Appl. Catal. A Gen.* **2016**, *522*, 54–69. [CrossRef]
16. Guo, R.; Wang, Q.; Pan, W.; Chen, Q.; Ding, H.; Yin, X.; Yang, N.; Lu, C.; Wang, S.; Yuan, Y. The poisoning effect of heavy metals doping on Mn/TiO_2 catalyst for selective catalytic reduction of NO with NH_3. *J. Mol. Catal. A Chem.* **2015**, *407*, 1–7. [CrossRef]
17. Jeevahan, J.; Mageshwaran, G.; Joseph, G.B.; Raj, R.B.D.; Kannan, R.T. Various strategies for reducing No x emissions of biodiesel fuel used in conventional diesel engines: A review. *Chem. Eng. Commun.* **2017**, *204*, 1202–1223. [CrossRef]
18. Liang, L.; Hui, S.; Pan, S.; Shang, T.; Liu, C.; Wang, D. Influence of mixing, oxygen and residence time on the SNCR process. *Fuel* **2014**, *120*, 38–45. [CrossRef]
19. Nam, C.M.; Gibbs, B.M. Selective non-catalytic reduction of NO_x under diesel engine conditions. *Proc. Combust. Inst.* **2000**, *28*, 1203–1209. [CrossRef]
20. Haputhanthri, S.O.; Maxwell, T.T.; Fleming, J.; Austin, C. Ammonia and Gasoline Fuel Blends for Spark Ignited Internal Combustion Engines. *J. Energy Resour. Technol.* **2015**, *137*, 062201. [CrossRef]
21. Valera-Medina, A.; Xiao, H.; Owen-Jones, M.; David, W.I.F.; Bowen, P.J. Ammonia for power. *Prog. Energy Combust. Sci.* **2018**, *69*, 63–102. [CrossRef]
22. Ryu, K.; Zacharakis-Jutz, G.E.; Kong, S.-C. Performance characteristics of compression-ignition engine using high concentration of ammonia mixed with dimethyl ether. *Appl. Energy* **2014**, *113*, 488–499. [CrossRef]
23. Mørch, C.S.; Bjerre, A.; Gøttrup, M.P.; Sorenson, S.C.; Schramm, J. Ammonia/hydrogen mixtures in an SI-engine: Engine performance and analysis of a proposed fuel system. *Fuel* **2011**, *90*, 854–864. [CrossRef]
24. Ryu, K.; Zacharakis-Jutz, G.E.; Kong, S.-C. Effects of gaseous ammonia direct injection on performance characteristics of a spark-ignition engine. *Appl. Energy* **2014**, *116*, 206–215. [CrossRef]
25. Lee, D.; Song, H.H. Development of combustion strategy for the internal combustion engine fueled by ammonia and its operating characteristics. *J. Mech. Sci. Technol.* **2018**, *32*, 1905–1925. [CrossRef]
26. Reiter, A.J.; Kong, S.-C. Combustion and emissions characteristics of compression-ignition engine using dual ammonia-diesel fuel. *Fuel* **2011**, *90*, 87–97. [CrossRef]
27. He, F.; Li, S.; Yu, X.; Du, Y.; Zuo, X.; Dong, W.; Sun, P.; He, L. Comparison study and synthetic evaluation of combined injection in a spark ignition engine with hydrogen-blended at lean burn condition. *Energy* **2018**, *157*, 1053–1062. [CrossRef]
28. Wang, Y.; Yu, X.; Ding, Y.; Du, Y.; Chen, Z.; Zuo, X. Experimental comparative study on combustion and particle emission of n-butanol and gasoline adopting different injection approaches in a spark engine equipped with dual-injection system. *Fuel* **2018**, *211*, 837–849. [CrossRef]
29. Convergent Science Corp. *Converge Theory Manual*; Convergent Science Corp: Madison, WI, USA, 2016.
30. Senecal, P.K.; Pomraning, E.; Richards, K.J.; Briggs, T.E.; Choi, C.Y.; Mcdavid, R.M.; Patterson, M.A. Multi-Dimensional Modeling of Direct-Injection Diesel Spray Liquid Length and Flame Lift-off Length using CFD and Parallel Detailed Chemistry. *SAE Trans.* **2003**, *112*, 1331–1351.
31. Liu, Y.-D.; Jia, M.; Xie, M.-Z.; Pang, B. Enhancement on a Skeletal Kinetic Model for Primary Reference Fuel Oxidation by Using a Semidecoupling Methodology. *Energy Fuels* **2012**, *26*, 7069–7083. [CrossRef]
32. Yang, J.; Ji, C.; Wang, S.; Wang, D.; Ma, Z.; Ma, L. A comparative study of mixture formation and combustion processes in a gasoline Wankel rotary engine with hydrogen port and direct injection enrichment. *Energy Convers. Manag.* **2018**, *168*, 21–31. [CrossRef]

33. Yang, J.; Ji, C.; Wang, S.; Wang, D.; Ma, Z.; Zhang, B. Numerical investigation on the mixture formation and combustion processes of a gasoline rotary engine with direct injected hydrogen enrichment. *Appl. Energy* **2018**, *224*, 34–41. [CrossRef]
34. Yang, J.; Ji, C.; Wang, S.; Zhang, Z.; Wang, D.; Ma, Z. Numerical investigation of the effects of hydrogen enrichment on combustion and emissions formation processes in a gasoline rotary engine. *Energy Convers. Manag.* **2017**, *151*, 136–146. [CrossRef]
35. Tao, F.; Golovitchev, V.I.; Chomiak, J. Self-Ignition and Early Combustion Process of n-Heptane Sprays Under Diluted Air Conditions: Numerical Studies Based on Detailed Chemistry. *SAE Trans.* **2000**, *109*, 2837–2854.
36. Kaminaga, T.; Kusaka, J.; Ishii, Y. A three-dimensional numerical study on exhaust gas emissions from a medium-duty diesel engine using a phenomenological soot particle formation model combined with detailed chemistry. *Int. J. Engine Res.* **2008**, *9*, 283–296. [CrossRef]
37. An, H.; Yang, W.M.; Li, J.; Zhou, D.Z. Modeling study of oxygenated fuels on diesel combustion: Effects of oxygen concentration, cetane number and C/H ratio. *Energy Convers. Manag.* **2015**, *90*, 261–271. [CrossRef]
38. Huang, H.; Lv, D.; Zhu, J.; Chen, Y.; Zhu, Z.; Pan, M.; Huang, R.; Jia, C. Development and Validation of a New Reduced Diesel/ n -Pentanol Mechanism for Diesel Engine Applications. *Energy Fuels* **2018**, *32*, 9934–9948. [CrossRef]
39. Golovitchev, V.I.; Montorsi, L.; Denbratt, I. Numerical Evaluation of a New Strategy of Emissions Reduction by Urea Direct Injection for Heavy Duty Diesel Engines. *Eng. Appl. Comput. Fluid Mech.* **2007**, *1*, 189–206. [CrossRef]
40. Baleta, J.; Mikulčić, H.; Vujanović, M.; Petranović, Z.; Duić, N. Numerical simulation of urea based selective non-catalytic reduction deNO$_x$ process for industrial applications. *Energy Convers. Manag.* **2016**, *125*, 59–69. [CrossRef]
41. An, H.; Yang, W.M.; Li, J.; Zhou, D.Z. Modeling analysis of urea direct injection on the NO x emission reduction of biodiesel fueled diesel engines. *Energy Convers. Manag.* **2015**, *101*, 442–449. [CrossRef]
42. Hiroyasu, H.; Kadota, T.; Arai, M. Development and Use of a Spray Combustion Modeling to Predict Diesel Engine Efficiency and Pollutant Emissions: Part 1 Combustion Modeling. *Bull. JSME* **1983**, *26*, 569–575. [CrossRef]
43. Han, Z.; Reitz, R.D. Turbulence Modeling of Internal Combustion Engines Using RNG κ-ε Models. *Combust. Sci. Technol.* **1995**, *106*, 267–295. [CrossRef]
44. Han, Z.; Reitz, R.D. A temperature wall function formulation for variable-density turbulent flows with application to engine convective heat transfer modeling. *Int. J. Heat Mass Transf.* **1997**, *40*, 613–625. [CrossRef]
45. Ricart, L.M.; Reltz, R.D.; Dec, J.E. Comparisons of Diesel Spray Liquid Penetration and Vapor Fuel Distributions With In-Cylinder Optical Measurements. *J. Eng. Gas Turbines Power* **2000**, *122*, 588. [CrossRef]
46. O'Rourke, P. Collective Drop Effects on Vaporizing Liquid Sprays. Ph.D. Thesis, Princeton University, Princeton, NJ, USA, 1981.
47. Shi, C.; Ji, C.; Wang, S.; Yang, J.; Ma, Z.; Ge, Y. Combined influence of hydrogen direct-injection pressure and nozzle diameter on lean combustion in a spark-ignited rotary engine. *Energy Convers. Manag.* **2019**, *195*, 1124–1137. [CrossRef]
48. Yin, Z.; Adamovich, I.V.; Lempert, W.R. OH radical and temperature measurements during ignition of H2-air mixtures excited by a repetitively pulsed nanosecond discharge. *Proc. Combust. Inst.* **2013**, *34*, 3249–3258. [CrossRef]
49. Chen, J.; Chen, Y. A study on heat release rate indicator in the auto-igniting droplets using direct numerical simulation. *J. Therm. Sci. Technol.* **2016**, *11*, JTST0008. [CrossRef]
50. Desantes, J.M.; García-Oliver, J.M.; Vera-Tudela, W.; López-Pintor, D.; Schneider, B.; Boulouchos, K. Study of the auto-ignition phenomenon of PRFs under HCCI conditions in a RCEM by means of spectroscopy. *Appl. Energy* **2016**, *179*, 389–400. [CrossRef]
51. O'Loughlin, W.; Masri, A.R. The Structure of the Auto-Ignition Region of Turbulent Dilute Methanol Sprays Issuing in a Vitiated Co-flow. *Flow Turbul. Combust.* **2012**, *89*, 13–35. [CrossRef]
52. Heywood, J.B. Pollutant formation and control in spark ignition engines. *Symp. Combust.* **1975**, *15*, 1191–1211. [CrossRef]
53. Alasfour, F.N. NO$_x$ Emission from a spark ignition engine using 30% Iso-butanol–gasoline blend: Part 1—Preheating inlet air. *Appl. Therm. Eng.* **1998**, *18*, 245–256. [CrossRef]

54. Miller, R.; Davis, G.; Lavoie, G.; Newman, C.; Gardner, T. A Super-Extended Zel'dovich Mechanism for NO_x Modeling and Engine Calibration. *SAE Trans.* **1998**, *107*, 1090–1100.
55. Kim, M.; Oh, J.; Lee, C. Study on Combustion and Emission Characteristics of Marine Diesel Oil and Water-In-Oil Emulsified Marine Diesel Oil. *Energies* **2018**, *11*, 1830. [CrossRef]
56. Taghavifar, H.; Anvari, S.; Parvishi, A. Benchmarking of water injection in a hydrogen-fueled diesel engine to reduce emissions. *Int. J. Hydrog. Energy* **2017**, *42*, 11962–11975. [CrossRef]
57. Boretti, A.; Osman, A.; Aris, I. Direct injection of hydrogen, oxygen and water in a novel two stroke engine. *Int. J. Hydrog. Energy* **2011**, *36*, 10100–10106. [CrossRef]
58. Lanzanova, T.D.M.; Dalla Nora, M.; Zhao, H. Performance and economic analysis of a direct injection spark ignition engine fueled with wet ethanol. *Appl. Energy* **2016**, *169*, 230–239. [CrossRef]
59. Sjöberg, M.; Dec, J.E. An investigation into lowest acceptable combustion temperatures for hydrocarbon fuels in HCCI engines. *Proc. Combust. Inst.* **2005**, *30*, 2719–2726. [CrossRef]